Materials Research. 2019; 22(4): e20180604
DOI: http://dx.doi.org/10.1590/1980-5373-MR-2018-0604

Influence of Zirconium Percentage on Microhardness and Corrosion Resistance of Ti_{50} $Ni_{50-x}Zr_x$ Shape Memory Alloys

Alana Pereira Ramos[a]*, ***Walman Benício de Castro***[b], ***Josiane Dantas Costa***[c],

Renato Alexandre Costa de Santana[d]

[a] *Departamento de Engenharia de Materiais, Universidade Federal de Campina Grande, Campina Grande, PB, Brasil.*
[b] *Departamento de Engenharia Mecânica, Universidade Federal de Campina Grande, Campina Grande, PB, Brasil.*
[c] *Departamento de Engenharia Quimica, Universidade Federal de Campina Grande, Campina Grande, PB, Brasil.*
[d] *Departamento de Biologia e Quimica, Universidade Federal de Campina Grande, Cuité, PB, Brasil.*

Received: September 04, 2018; Revised: December 20, 2018; Accepted: June 18, 2019

To obtain high temperature shape memory alloys of the lower cost Ni-Ti-X system, elements such as Hf and Zr are introduced to modify the thermal and mechanical properties of these alloys. This work studied the production and characterization of Ti_{50} Ni_{50-x} Zr_x alloys (x = 0, 5, 10 at.%) with the aim of improving their thermal, mechanical and corrosion resistance properties. In the resulting alloys, transformation of phase B2 into phase B19' occurred in a single stage. The addition of zirconium led to an increase of transformation temperatures, as well as the appearance of second phase particles in the grain boundaries of the matrix. The increase in zirconium percentage favored the increase of corrosion resistance from 520.23KΩ to 1007.30KΩ and of microhardness from 346HV to 543HV for the N0 and N10 alloys, respectively.

Keywords: *Ti-Ni-Zr alloys, corrosion, microhardness, shape memory.*

1. Introduction

More research is being conducted on Ni-Ti alloys, also known as Nitinol, because of their unusual properties[1-3]. they have high corrosion resistance, biocompatibility, shape memory effect and superelasticity. The use of such alloys as biomaterial has been increasing as their superelastic properties allow greater reversible deformations[2,4]. However, transformation temperatures of these alloys range from -100ºC to 100ºC, hence their application may be limited for industrial purposes[5,6].

A third element is added to increase the transformation temperature of alloys containing nickel titanium. An option for the third element to form the Ni-Ti-X alloy is Hafnium or Zirconium, usually ranging from 5 to 20%. These elements have been the focus of research because they are less expensive than Pd, Pt or Au, and they can increase the transformation temperature of Ni-Ti alloys[7,8]. Previous studies have reported an increase in characteristic transformation temperatures (M_s, M_f, A_s, A_f) with increased Hf or Zr content in these alloys[9-11].

The addition of zirconium can provide transformation temperatures of up to 200º C[10,12-14] for possible applications in gas turbines, rocket engines, automotive engines, and nuclear reactors. In most studies, zirconium is added to the solid solution to replace Ti, thus raising transformation temperatures and increasing hardness and corrosion resistance[5,11,15,16]. However, studies about the mechanical, corrosive and functional behavior of Ti-Ni-Zr alloys are still very limited. The addition of zirconium may also lead to the appearance of unknown secondary phases that directly influence the properties of these alloys[9-12,14].

The objectives of this work were to produce $Ti_{50}Ni_{50-x}Zr_x$ (x = 0, 5, 10) alloys through the *Plasma Skull Push-Pull* process and to investigate the influence of zirconium percentage on microstructure, transformation temperatures, microhardness and corrosion resistance.

2. Experimental Procedure

2.1 Production of alloys by Plasma Skull Push-Pull

Twenty grams of each alloy were produced using the *Plasma Skull Push-Pull* (PSPP) melting method, in which metal is melted in a copper cylinder and then injected into a cylindrical aluminum mold. This technique was implemented by Araújo et al.[17] for production of Ni-Ti alloys and Cu-based

---

*e-mail: alanapramos@yahoo.com.br

alloys. The study alloys were prepared with pure metals Ti (99.99%), Ni (99.97 %,) and Zr (99.99%), using a Discovery Plasma device, manufactured by *EDG Equipamentos e Controles*. During the melting process, the alloys were melted again at least five other times under an argon atmosphere. Through electrical discharge machining (EDM) at low current discharges, the samples were cut in the shape of disks (12.4 mm diameter). The nomenclature described in Table 1 was used to identify the alloys more easily.

Table 1. Nominal composition of Ti-Ni-Zr alloys in atomic weight

Alloys	Nominal (%at.) composition
N0	$Ti_{50}Ni_{50}$
N5	$Ti_{50}Ni_{45}Zr_{5}$
N10	$Ti_{50}Ni_{40}Zr_{10}$

2.2 Characterization of the alloys

Firstly, the alloys were analyzed by X-ray Diffraction (XRD) for phase identification with a Shimadzu 6100 diffractogram, using copper K-alpha radiation, 40 kV voltage and 30 mA operating current. Scanning range varied from 20° to 60°, using spectral slits of 5° and scanning speed of 0.02°C/min.

Transformation temperatures were determined by Differential Scanning Calorimetry (DSC) analysis on a Q20 DSC Calorimeter (DuPont). The tests were performed at a rate of 10°C/min. with high-purity argon flux during both heating and cooling, with temperature ranging between -60°C and 120°C for the Ti-Ni alloy, and from 0°C to 200°C for Ti-Ni-Zr alloys. Alumina crucibles were used as containers.

For analysis of microstructure and morphology, Scanning Electron Microscopy (SEM) analyses were carried out on a TESCAN VEGA 3SBH SEM microscope, with 20Kv voltage. Energy dispersive spectroscopy (EDS) was also used to collect data on alloy composition. Before SEM measurements, the samples were etched in a H_2O:HNO_3:HF 5:4:1 solution to reveal their microstructures.

To determine microhardness and modulus of elasticity, microhardness tests were performed on a Shimadzu DUH - 211S Dynamic Ultra Micro Hardness Tester. The test was performed with a load of 200 mN and penetration time of 20 seconds and the average of at least 5 readings was calculated.

The corrosion test was performed with a potentiostat, an electrochemical cell composed of an electrolyte (corrosive medium), a working electrode (study alloy), a reference electrode (saturated calomel electrode) and counter electrode (platinum electrode). The electrochemical cell was inserted into a Faraday cage to prevent any external disturbance from causing noise in the measurements. The tests were carried out with 3.5% NaCl (sodium chloride) solution as the corrosive medium, at room temperature, for simulation of sea water. The polarization curves were determined with a scanning rate of 1 mVs^{-1} using an Autolab PGSTATE 302N potentiostat/galvanostat connected to a computer by the software NOVA 1.11. Electrochemical impedance spectroscopy tests were performed on the same equipment used for potentiodynamic polarization, with frequency range from 100 kHz to 0.01 Hz and amplitude of 0.01 V. The input data used in this analysis consisted of the open-circuit potential values that were measured after 60 minutes.

3. Results and Discussion

X-ray diffraction was performed to identify the present phases, and these results are shown in Figure 1. Phase identification was based on ICDD International Centre for Diffraction Data. The patterns in Figure 1 show that all the alloys present the characteristic phases of the shape memory effect; the austenite phase FCC (B2) was found on planes (100),(101),(200) and the monoclinic martensite phase (B19'), on planes $(11\bar{1})$, (210), (111); similar identification was found by Hsieh & Wu[12] and Evirgen et al.[9]. Characteristic peaks of titanium oxides TiO_2(211) and TiO(202) were formed, and so were zirconium oxides (311), because these elements are highly reactive to oxygen, as also found by Hsieh et al.[18]. While Ti atoms migrate to form TiO_2 and TiO particles, residual Ni atoms diffuse into the TiNi matrix to form Ni-rich regions, and then the Ni_4Ti_3 $(22\bar{3})$ and $Ni_{10}Zr_7$ (422) phases appear[18,19]. Also in the N5 and N10 alloys, other phases appear, e.g., λ1 and NiZr phases and the coexistence of the austenite and martensite phases, which was also found by other authors[19,20]. Table 2 shows the transformation temperatures of these alloys.

Peaks shown in Figure 2 are identified as being associated with martensite (B19') and austenite (B2) transformation into Ti-Ni-Zr alloys[9,12,14]. The addition of zirconium led to a significant increase in martensite transformation temperatures, ranging from 2°C in the N0 alloy to 51°C in the N5 alloy. The increase in Zr percentage caused peak displacement to the right, raising the austenite transformation temperatures from 80°C for the N5 alloy to 93°C for the N10 alloy. Reasons for this increase are changes in matrix composition, appearance of secondary phases, as seen in the diffractogram (Figure 1), and the fact that these are Ti-rich Ti-Ni-Zr alloys, since transformation temperatures can also increase as the content (Ti + Zr) increases to 51.5%, as found by Hsieh and Wu[11,12,14]. The decrease of M_s temperature of the N10 alloy can also be due to the variation of mean valence electrons per atom (ev/a) and to valence electron concentration (VEC) in the matrix, as a result of the large amount of Zr. A similar result was found in studies using Ti-Ni-Cu-Zr-based alloys and different zirconium percentages: additions of up to 5% Zr can decrease transformation temperatures[21]. These temperatures are still considered to be high because the alloys are as-cast samples, and alloys of the same system, when studied by Evirgen et al.[9] only presented similar or higher temperatures

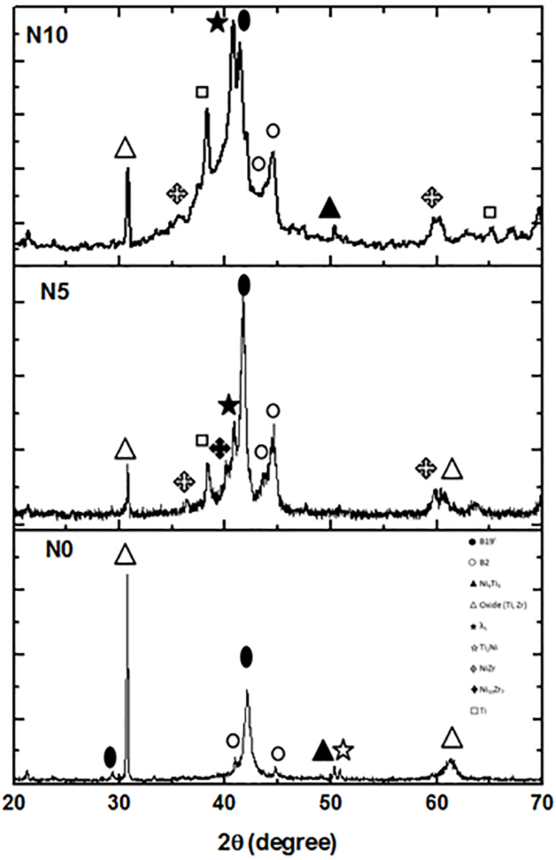

Figure 1. Diffractograms of the alloys N0, N5 e N10.

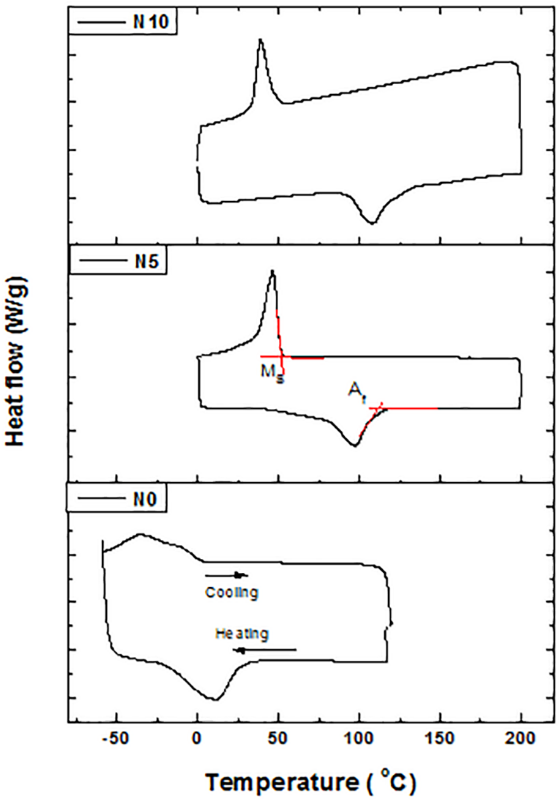

Figure 2. DSC curves of the alloys, N0 alloy (a), N5 alloy (b), N10 alloy (c). The temperatures As and Ms were obtained by the tangent method as shown in the curve of Fig. (b).

Table 2. Phase Transformation Temperatures

Alloys	M_s (°C)	M_p (°C)	M_f (°C)	A_s (°C)	A_p (°C)	A_f (°C)
N0	2	-33	-51	-20	11	25
N5	51	46	36	80	98	109
N10	48	38	34	93	108	120

after heat treatment at 550°C for 10 hours. When Wu and Hsieh[16] carried out studies with Ti-Ni-Zr alloys, they found that M_s transformation temperatures decrease to approximately 50ºC as hardness increases, because of the shear restriction caused by increased hardness. Based on the results shown in Figure 2 and Table 2, it can be stated that an Ti-Ni-Zr alloy can be obtained with the desired transformation temperatures by carefully controlling the percentage of Zr.

Figures 3(a-b) show micrographs of the N0 alloy, in Fig. 3a it is possible to observe the formation of more defined grains of the matrix phase composed of NiTi (composition described in Table 3), in Fig. 2b it is observed the presence of a precipitate with a size of about 20 µm, dispersed in the N0 alloy matrix and several other minor precipitates. The EDS analyzes (Table 3) on the matrix and the precipitates show that the composition of the matrix is almost equiatomic and precipitates are mainly composed of titanium[22]. Figure 3 (c-d) shows the micrographs of N5 alloy where it is possible to observe a large number of particles of the second phase around the grain boundaries of the matrix phase (Ti, Zr), Ni, this second phase is probably the second phase $(Ti, Zr)_2$, Ni, as it was observed or by other authors[14,16]. The compositions of these phases are described in Table 3. In Fig. 3d it is possible to observe that some particles of the second phase are trapped in the matrix that phenomenon was also observed in other works[14,16]. Figure 3e shows the micrograph of N10 alloy where the presence of two phases is observed (composition described in Table 3). The matrix phase (Ti, Zr), Ni[14,16,23] and the grain growth of the second phase (about 10 µm) with more defined polygonal shapes; a similar result was observed by Khan et al., 2017. With the addition of Zr there was the emergence of other phases, as shown in Figs. 3c-y confirming the results obtained by DRX (Fig. 1). The investigations carried out also reveal that NiTiZr shape memory alloys always show secondary phases[14,16,23,24].

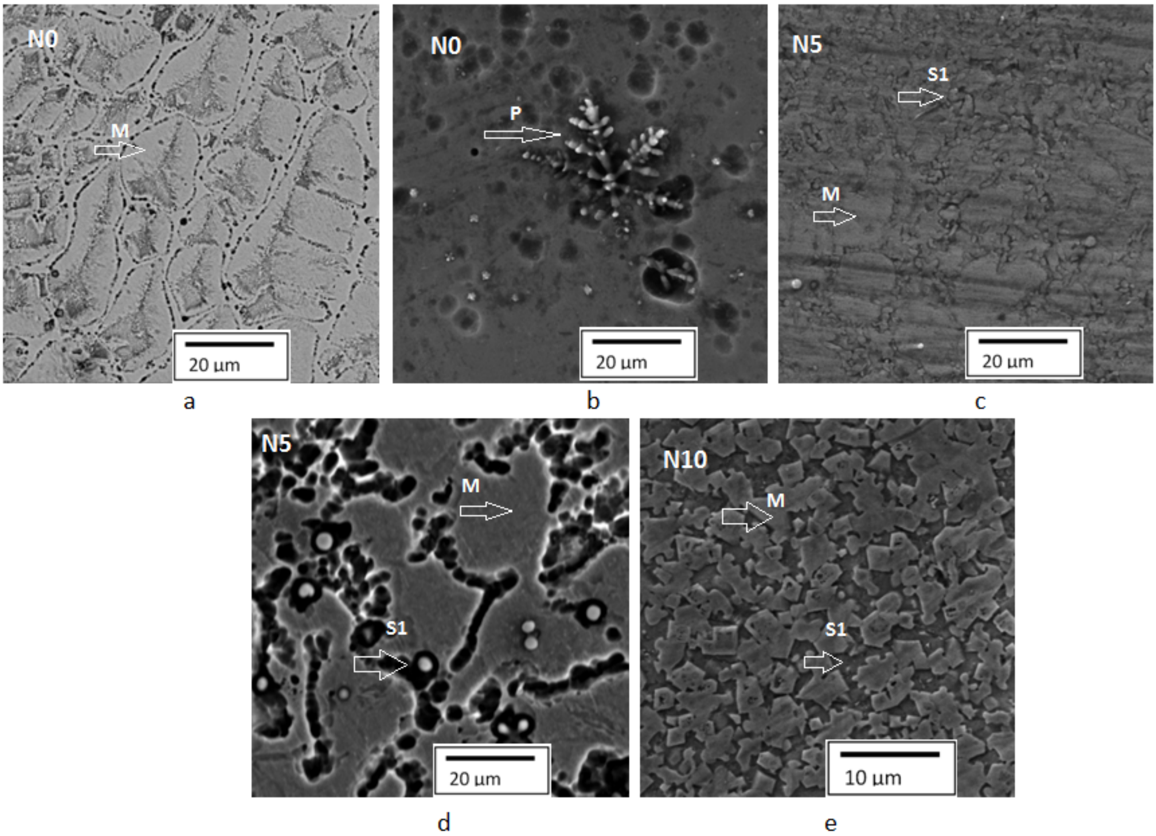

Figure 3. Scanning electron microscopy of the alloys N0 (a-b), N5 (c-d) and N10 (e), respectively. Legend: M: matrix, P: precipitate, S1: second phase.

Table 3. Chemical composition of the phases obtained by EDS.

Alloys		**Chemical Composition (at%)**		
		Ti	**Ni**	**Zr**
N0	Matrix	51,7 ± 0,5	48,2 ± 0,5	0
	Second phase	79,4 ± 2,2	20,5 ± 2,2	0
N5	Matrix	48,9 ± 0,9	46,7 ± 0,5	4,3 ± 1,4
	second phase	54,6 ±1,8	37,9 ± 1,5	7,4 ± 2,6
N10	Matrix	51,3 ± 2,8	34,9 ± 1,5	13,8 ± 4,3
	Second phase	45,9 ± 0,1	46,4 ± 0,5	7,7 ± 0,5

The nanoindentation method for obtantion hardness and modulus of elasticity has already been used by other authors[25,26]. Table 4 shows the modulus of elasticity and microhardness (HV) measurements for alloys N0, N5 and N10. Figure 4 shows the images captured after indentation was performed in each phase, as specified in Table 4. There was a clear effect of adding zirconium to the alloys, namely, an increase in the values of microhardness and modulus of elasticity. The highest values of microhardness were found in the alloy with 10% zirconium. This increase was already expected, because when zirconium is added, a solid solution is formed and it increases hardness. The reason is that zirconium has a larger atomic radius than titanium and nickel, thus causing distortions in crystal lattices which prevent disorder and result in increased microhardness and formation of the Ni_4Ti_3 phase. This result was also found by Firstov et al.[15] in their work. Table 4 shows the variation in the values of microhardness and modulus of elasticity when there is variation in chemical composition in each phase.

In the N0 alloy, analyses were made of the matrix and on the light (P1) and dark (P2) particles. There was not enough variation to allow the conclusion that they are different phases. Because indentation cannot be performed only on the particles, the obtained value is only tentative, since part of the indentation occurs in the matrix phase. However, it can be claimed that these precipitates are harder than the matrix,

Table 4. Microhardness and modulus of elasticity of the alloys ($Ti_{50}Ni_{50-x}Zr_x$).

Alloys	Phase	Microhardness (HV)	Modulus of elasticity (GPa)
N0	Matrix	346 ± 2	57 ± 1
	Second phase (S1)	407 ± 4	63 ± 8
N5	Matrix	319 ± 15	66 ± 4
	Second phase (S1)	614 ± 19	82 ± 3
N10	Matrix	543 ± 27	95 ± 2
	Second phase (S1)	762 ± 15	92 ± 5

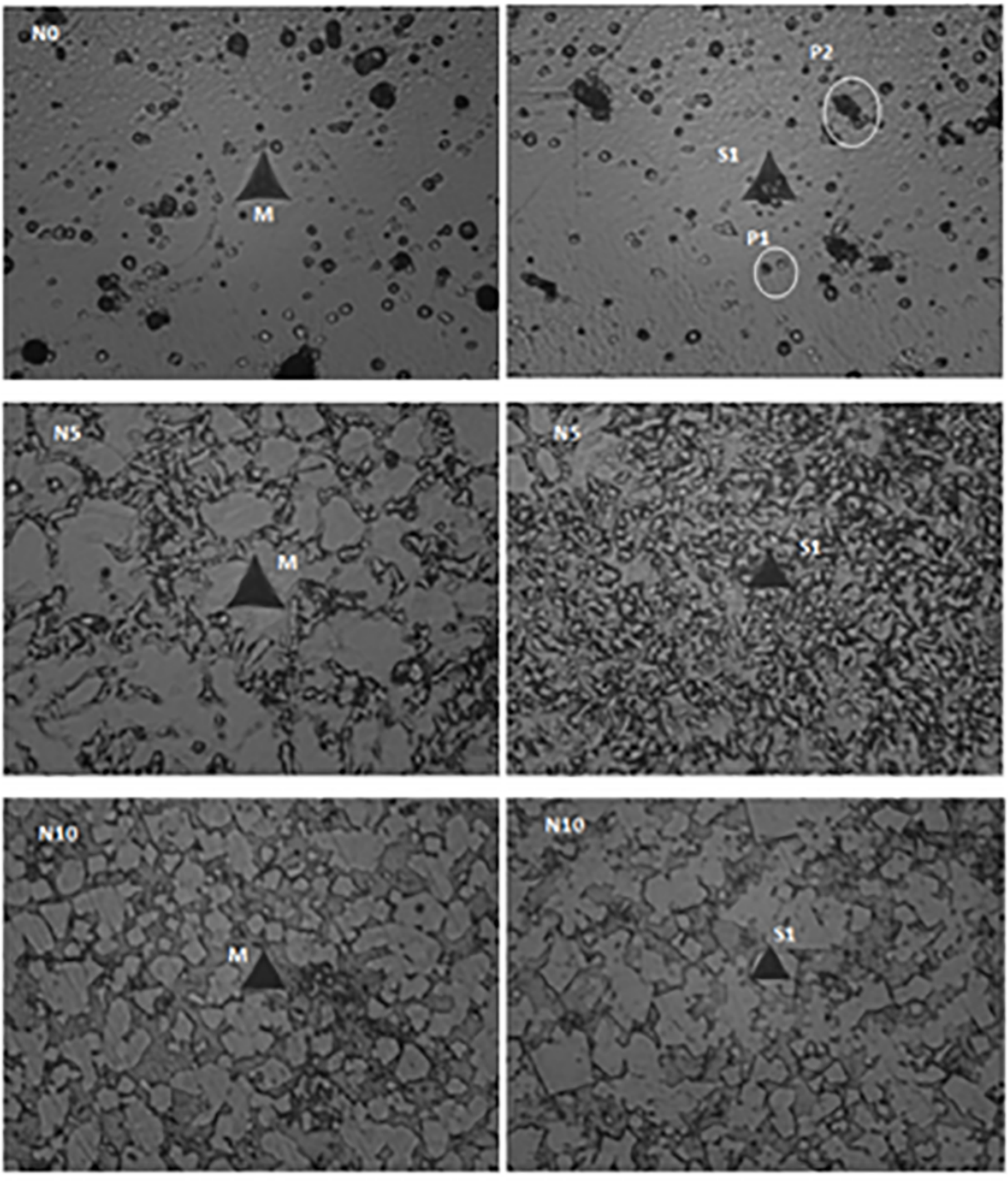

Figure 4. Indents made on the N0, N5 and N10 alloys. M: matrix, P1: precipitate light color, P2: precipitate dark color, S1: second phase.

because the obtained values were higher. These particles can be precipitated from the Ni_4Ti_3 phase, which increases the hardness of the alloy and also make difficult the slippage of the discordances[27]. The formation of oxides such as TiO_2, TiO, as shown in the diffractograms of Figure 1, also favors alloy hardening[28]. In the N5 alloy, the second phase that appears in the grain boundary has a higher microhardness value (614 HV) because this phase is enriched by adding zirconium, according to the composition shown in Table 4. In the N10 alloy, hardness of the second phase is greater than that of the matrix phase; up to 762 HV. This high level of hardness may be the reason why martensite transformation temperatures are still below 100°C, since any strengthening mechanism that prevents shear can decrease transformation temperatures, because martensite transformation involves a shear process[12,14].

Table 4 shows the modulus of elasticity values of the alloys. In general, modulus of elasticity values are increased as microhardness increases in all the alloys. This behavior may be associated to changes in the microstructures as observed in XRD and SEM. The highest modulus of elasticity value was identified in the N10 alloy (95 GPa) and the lowest value in the N0 alloy (57 GPa). This high modulus of elasticity value indicates that the N10 alloy is the greater rigidity.

Electrochemical measurements were performed to evaluate the effect of zirconium addition on corrosion resistance of Ti-Ni-Zr alloys. Figure 5 shows the behavior of the open-circuit potential (OCP) as a function of time. At the beginning, there was an increase followed by a decrease in the OCP value, which may be due to the formation and dissolution of the passive film until it reached stability. The increase of zirconium percentage in the alloy shifted OCP potentials to positive values. This means that the increase of zirconium in the alloy favors the formation of oxide at the electrode/electrolyte interface, which results in higher OCP values. Thus, the increase of zirconium content led to an increase of oxide thickness and, consequently, of the more stable passive layer. The oxides which are formed may be TiO, TiO_2 and Ti_2ZrO. After the increase of zirconium content, the alloy becomes more resistant to corrosion, as far as thermodynamic parameters are concerned[29,30].

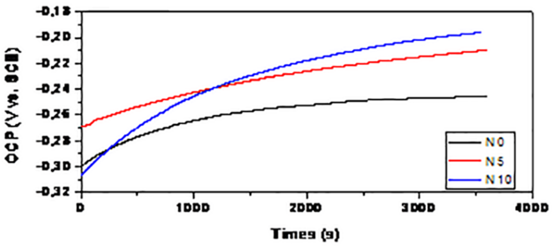

Figure 5. OCP curves of N0, N5 and N10 alloys.

Figure 6 shows the linear potentiodynamic polarization curves (PPL). For corrosion measurements, the Tafel extrapolation method was used to determine potential corrosion values (E_{Corr}), corrosion current (j_{Corr}), resistance to polarization (Rp) and anodic (ba) and cathodic (bc) Tafel coefficients. Table 5 shows the values obtained by the Tafel extrapolation method. Calculation of the corrosion current was based on the Stern-Geary equation[31,32]:

$$ICorr = \frac{b_a \cdot b_c}{2.3(b_a + b_c)R_p} \tag{1}$$

where *ba* and *bc* represent the slopes of the anodic and cathodic Tafel's equations, respectively, and ICorr represents the corrosion current.

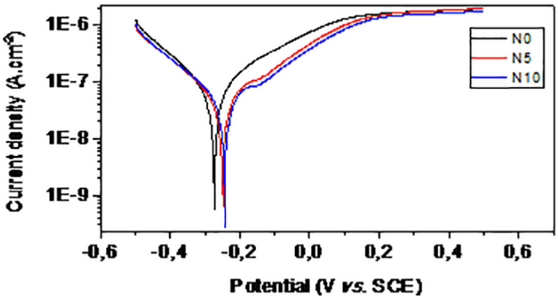

Figure 6. Potentiodynamic polarization curves for N0, N5 and N10 alloys obtained in 3.5 NaCl.

The hydrogen evolution reaction usually occurs by the polarization curves, in the cathodic region, because the solution is aqueous, while metal dissolution/passivation and oxygen evolution occur in the anodic region[33,34]. When zirconium content increased, the corrosion potential was shifted to positive values. This was the same behavior found for the OCP results. A passivation film was formed in the N5 and N10 alloys, starting at the potential -0.183V and ending at the potential -0.131V. When the potential value increase, the passive film was broken down. The passive film formed by the N10 alloy is more stable than the one formed by the N5 alloy. This behavior may be due to the increase of zirconium in the alloy and, consequently, the fact that zirconium oxides reacted with titanium oxides (TiO_2, TiO)[8,35], as shown in the XRD diffractograms (Figure 1). This oxide layer increased the strength of the alloy by forming a barrier between the metal and the solution, thereby reducing nickel oxidation[36]. The increase of zirconium content brought about microstructural changes which favored increased hardness and may have affected corrosion resistance. The studies by Balcerzak[8], reported a similar result: after Zr was added to

Table 5. Results obtained by the linear potentiodynamic polarization of the N0, N5 and N10 alloys.

Alloys	E_{corr} (mV)	j_{corr} (nA/cm^2)	R_p (KΩ.cm^2)	ba (mV.dec^{-1})	-bc (mV.dec^{-1})
N0	-272.95	147.00	520.23	281.65	358.94
N5	-251.16	60.89	928.87	212.11	271.78
N10	-244.18	52.42	1007.30	202.05	270.65

the Ni-Ti alloy, there was an increase of corrosion resistance. When Zr is introduced into the alloy, there is a change in the unit cell volume by replacing Ti with Zr, which has a larger atomic radius. This replacement causes phase changes in the resulting material, which favors the increase of corrosion resistance of the Ni-Ti alloy[8].

The results for the polarization curves show that the addition of zirconium caused an increase in corrosion resistance, reaching 1007.30 KΩ.cm^2 for the N10 alloy, i.e., an increase of approximately 40% (Table 5).

In order to confirm the results of the polarization test, the electrochemical impedance spectroscopy (EIS) test was performed and the results are shown as a diagram of Nyquist in Figure 7. As the arc increases, there is an increase in impedance values, that is, in the corrosion resistance of Ni-Ti-Zr alloys. The diagrams suggest a typical capacitive behavior of passive materials, involving a protective film with high corrosion resistance.

An equivalent circuit was proposed to simulate the behavior of the Nyquist diagrams (Figure 8). The equivalent circuit that was used is the simplest, known as Randles circuit[37-39]. The equivalent circuit consists of the following elements: Rs - solution resistance, Rp - passive film polarization resistance and charge transfer resistance (Rct). Rct is the constant phase element which represents passive film capacitance. Rct is inserted from the equivalent circuit to replace a pure capacitor in order to improve the fit of the proposed model[40,41]. Table 6 shows the results of the proposed equivalent circuit fitting. The solution resistance value (Rs) was approximately 81 Ω.cm^2, which shows that all the experiments were performed with the same initial conditions.

The N5 and N10 alloys present a passive behavior and have higher corrosion resistance, which confirms the results for the polarization curves. Figure 7 shows the experimental

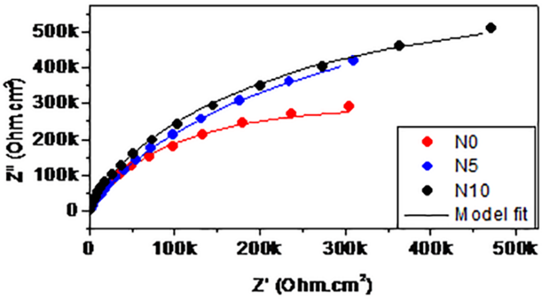

Figure 7. Nyquist diagram for the N0, N5 and N10 alloys obtained in open circuit potential.

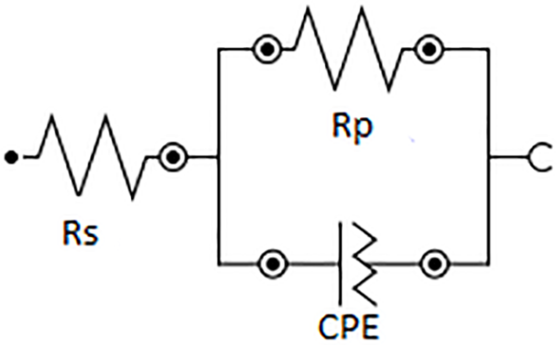

Figure 8. Equivalent electrical circuit used to adjust the experimental data of the impedance spectra.

Table 6. Adjusted parameters of the equivalent circuit for Ni-Ti-Zr alloys

Alloys	Rs (Ω.cm^2)	CPE (µF.cm^{-2})	*n*	Rp (MΩ.cm^2)
N0	81.70	5.66	0.90	0.65
N5	81.40	0.16	0.84	1.33
N10	81.80	0.16	0.85	1.44

data for the *Nyquist* curves. The corrosion resistance of the N5 alloy may be associated with grain refinement of alloy, because the corrosion resistance of NiTi alloys depends on grain size; fine grains favor the formation of a more noble and more compact passive film when there are larger amounts of grain boundaries, working as nucleation sites for the passive film[42-44]. The increase of Zr content in the alloy results in a decreased formation of TiO_2 and increased formation of zirconium oxide, because zirconium oxides are more compact than titanium oxides, hence corrosion resistance is improved[41]. The presence of Ni_4Ti_3 particles also favors the increase of corrosion resistance , since they increased the Ti/Ni ratio in the matrix and the formation of oxides (TiO)[45].

4. Conclusion

The present study focused on the characteristics of ternary shape memory alloys (Ti-Ni-Zr) and important conclusions have been drawn:

In these alloys, transformation of phase B2 into phase B19' occurs in a single stage and Ms and As temperatures increase from 2ºC to 48ºC and from -20ºC to 93ºC for N0 and N10 alloys, respectively.

Addition of zirconium caused the appearance of second phase particles in the grain boundaries of the N5 and N10 alloy matrix. In addition, it increased corrosion resistance from 520.23KΩ to 1007.30KΩ for N0 and N10 alloys, respectively, and increased microhardness from 346HV (N0) to 543HV (N10). In the second phase, there was even greater hardness, reaching 762HV, while modulus of elasticity was 92 GPa.

The increase in Zr content in the alloy caused a change in its microstructure and hence in the electro-electrolyte interface, which favored the formation of Zr oxides which increased the corrosion resistance of the resulting alloys.

5. Acknowledgements

To the Coordenação de Aperfeiçoamento de Pessoal de Nível Superior - CAPES (Coordination for Improvement of Higher Education Personnel) for granting the graduate scholarship.

6. References

1. Flamini DO, Valle MI, Sandoval MJ, Massheimer VL, Saidman SB. Electrodeposition study of polypyrrole-heparin and polypyrrole-salicylate coatings on Nitinol. *Materials Chemistry and Physics*. 2018;209:76-85.

2. Nagaraja S, Sullivan SJL, Stafford PR, Lucas AD, Malkin E. Impact of nitinol stent surface processing on in-vivo nickel release and biological response. *Acta Biomaterialia*. 2018;72:424-433.

3. Duerig T. The metallurgy of Nitinol as it pertains to medical devices. In: Froes FH, Qian MA, eds. *Titanium in Medical and Dental Applications*. Oxford: Woodhead Publishing; 2018. p. 555-570.

4. Lukina E, Kollerov M, Meswania J, Khon A, Panin P, Blunn GW. Fretting corrosion behavior of nitinol spinal rods in conjunction with titanium pedicle screws. *Materials Science and Engineering: C*. 2017;72:601-610.

5. Kim HY, Mizutani M, Miyazaki S. Crystallization process and shape memory properties of Ti-Ni-Zr thin films. *Acta Materialia*. 2009;57(6):1920-1930.

6. Shaw JA, Kyriakides S. Thermomechanical aspects of NiTi. *Journal of the Mechanics and Physics of Solids*. 1995;43(8):1243-1281.

7. Ma J, Karaman I, Noebe RD. High temperature shape memory alloys. *International Materials Reviews*. 2010;55(5):257-315.

8. Balcerzak M. Electrochemical and structural studies on Ti-Zr-Ni and Ti-Zr-Ni-Pd alloys and composites. *Journal of Alloys and Compounds*. 2016;658:576-587.

9. Evirgen A, Karaman I, Pons J, Santamarta R, Noebe RD. Role of nano-precipitation on the microstructure and shape memory characteristics of a new $Ni_{50.3}Ti_{34.7}Zr_{15}$ shape memory alloy. *Materials Science and Engineering: A*. 2016;655:193-203.

10. Evirgen A, Karaman I, Santamarta R, Pons J, Noebe RD. Microstructural characterization and superelastic response of a $Ni_{50.3}Ti_{29.7}Zr_{20}$ high-temperature shape memory alloy. *Scripta Materialia*. 2014;81:12-15.

11. Hsieh SF, Wu SK. A Study on Ternary Ti-rich TiNiZr Shape Memory Alloys. *Materials Characterization*. 1998;41(4):151-162.

12. Hsieh SF, Wu SK. A study on lattice parameters of martensite in $Ti_{50.5-x}Ni_{49.5}Zr_x$ shape memory alloys. *Journal of Alloys and Compounds*. 1998;270(1-2):237-241.

13. Cesari E, Ochin P, Portier R, Kolomytsev V, Koval Y, Pasko A, et al. Structure and properties of Ti-Ni-Zr and Ti-Ni-Hf melt-spun ribbons. *Materials Science and Engineering: A*. 1999;273-275:738-744.

14. Hsieh SF, Wu SK. Room-temperature phases observed in $Ti_{53-x}Ni_{47}Zr_x$ high-temperature shape memory alloys. *Journal of Alloys and Compounds*. 1998;266(1-2):276-282.

15. Firstov GS, Van Humbeeck J, Koval YN. High-temperature shape memory alloys: some recent developments. *Materials Science and Engineering: A*. 2004;378(1-2):2-10.

16. Wu SK, Hsieh SF. Martensitic transformation of a Ti-rich $Ti_{40.5}Ni_{49.5}Zr_{10}$ shape memory alloy. *Journal of Alloys and Compounds*. 2000;297(1-2):294-302.

17. de Araújo CJ, Gomes AAC, Silva JA, Cavalcanti AJT, Reis RPB, Gonzalez CH. Fabrication of shape memory alloys using the plasma skull push-pull process. *Journal of Materials Processing Technology*. 2009;209(7):3657-3664.

18. Hsieh SF, Hsue AWJ, Chen SL, Lin MH, Ou KL, Mao PL. EDM surface characteristics and shape recovery ability of $Ti_{35.5}Ni_{48.5}Zr_{16}$ and $Ni_{60}Al_{24.5}Fe_{15.5}$ ternary shape memory alloys. *Journal of Alloys and Compounds*. 2013;571:63-68.

19. Meisner LL, Sivokha VP, Perevalova OB. Formation features of fine structure of the $Ni_{50}Ti_{40}Zr_{10}$ alloy under different thermal treatment. *Physica B: Condensed Matter*. 1999;262(1-2):49-54.
20. Terayama A, Nagai K, Kyogoku H. Fabrication of Ti-Ni-Zr Shape Memory Alloy by P/M Process. *Materials Transactions*. 2009;50(10):2446-2450.
21. Li J, Yi X, Sun K, Sun B, Gao W, Wang H, et al. The effect of Zr on the transformation behaviors, microstructure and the mechanical properties of Ti-Ni-Cu shape memory alloys. *Journal of Alloys and Compounds*. 2018;747:348-353.
22. Frenzel J, Zhang Z, Somsen C, Neuking K, Eggeler G. Influence of carbon on martensitic phase transformations in NiTi shape memory alloys. *Acta Materialia*. 2007;55(4):1331-1341.
23. Guiose B, Cuevas F, Décamps B, Percheron-Guégan A. Solid-gas and electrochemical hydrogenation properties of pseudo-binary (Ti,Zr)Ni intermetallic compounds. *International Journal of Hydrogen Energy*. 2008;33(20):5795-5800.
24. Khan AN, Muhyuddin M, Wadood A. Development and characterization of Nickel-Titanium-Zirconium shape memory alloy for engineering applications. *Russian Journal of Non-Ferrous Metals*. 2017;58(5):509-515.
25. Yan FK, Zhang BB, Wang HT, Tao NR, Lu K. Nanoindentation characterization of nano-twinned grains in an austenitic stainless steel. *Scripta Materialia*. 2016;112:19-22.
26. Kim SW, Jo JW, Park CH, Hong JK, Yeom JT, Kim HG. Fracture toughness of TiNiHf alloys: A hybrid study using in-situ transmission electron microscopy experiments and finite element analyses. *Materials Science and Engineering: A*. 2016;655:363-372.
27. Otsuka K, Ren X. Physical metallurgy of Ti-Ni-based shape memory alloys. *Progress in Materials Science*. 2005;50(5):511-678.
28. Chen SL, Hsieh SF, Lin HC, Lin MH, Huang JS. Electrical discharge machining of TiNiCr and TiNiZr ternary shape memory alloys. *Materials Science and Engineering: A*. 2007;445-446:486-492.
29. Lethabane ML, Olubambi PA, Chikwanda HK. Corrosion behaviour of sintered Ti-Ni-Cu-Nb in 0.9% NaCl environment. *Journal of Materials Research and Technology*. 2015;4(4):367-376.
30. Li K, Li Y, Huang X, Gibson D, Zheng Y, Liu J, et al. Surface microstructures and corrosion resistance of Ni-Ti-Nb shape memory thin films. *Applied Surface Science*. 2017;414:63-67.
31. Costa JD, de Sousa MB, Fook NCML, Alves JJN, de Araújo CJ, Prasad S, et al. Obtaining and characterization of Ni-Ti/Ti-Mo joints welded by TIG process. *Vacuum*. 2016;133:58-69.
32. Costa JD, de Sousa MB, Alves JJN, Evaristo BO, Queiroga RA, dos Santos AX, et al. Effect of Electrochemical Bath Composition on the Preparation of Ni-W-Fe-P Amorphous Alloy. *International Journal of Electrochemical Science*. 2018;13:2969-2985.
33. Liu Y, Ren Z, Bai L, Zong M, Gao A, Hang R, et al. Relationship between Ni release and cytocompatibility of Ni-Ti-O nanotubes prepared on biomedical NiTi alloy. *Corrosion Science*. 2017;123:209-216.
34. Wang L, Chen M, Liu H, Jiang C, Ji V, Moreira F. Optimisation of microstructure and corrosion resistance of Ni-Ti composite coatings by the addition of CeO_2 nanoparticles. *Surface and Coatings Technology*. 2017;331:196-205.
35. Hang R, Liu Y, Bai L, Zong M, Wang X, Zhang X, et al. Electrochemical synthesis, corrosion behavior and cytocompatibility of Ni-Ti-O nanopores on NiTi alloy. *Materials Letters*. 2017;202:5-8.
36. Cissé O, Savadogo O, Wu M, Yahia LH. Effect of surface treatment of NiTi alloy on its corrosion behavior in Hanks' solution. *Journal of Biomedical Materials Research*. 2002;61:339-345.
37. Abu-Sharkh S, Doerffel D. Rapid test and non-linear model characterisation of solid-state lithium-ion batteries. *Journal of Power Sources*. 2004;130(1-2):266-274.
38. Haeri M, Goldberg S, Gilbert JL. The voltage-dependent electrochemical impedance spectroscopy of CoCrMo medical alloy using time-domain techniques: Generalized Cauchy-Lorentz, and KWW-Randles functions describing non-ideal interfacial behaviour. *Corrosion Science*. 2011;53(2):582-588.
39. Stróz A, Losiewicz B, Zubko M, Chmiela B, Balin K, Dercz G, et al. Production, structure and biocompatible properties of oxide nanotubes on Ti13Nb13Zr alloy for medical applications. *Materials Characterization*. 2017;132:363-372.
40. Zhao Y, Jiang C, Xu Z, Cai F, Zhang Z, Fu P. Microstructure and corrosion behavior of Ti nanoparticles reinforced Ni-Ti composite coatings by electrodeposition. *Materials & Design*. 2015;85:39-46.
41. Qiu ZK, Zhang PZ, Wei DB, Wei XF, Chen XH, Wang Y. Mechanical and electrochemical properties of Zr and Zr-Er alloyed layers deposited on titanium alloy (TC11). *Surface and Coatings Technology*. 2015;280:301-307.
42. Liu KT, Duh JG. Grain size effects on the corrosion behavior of $Ni_{50.5}Ti_{49.5}$ and $Ni_{45.6}Ti_{49.3}Al_{5.1}$ films. *Journal of Electroanalytical Chemistry*. 2008;618(1-2):45-52.
43. Liu JC, Zhang G, Nagao S, Jiu JT, Nogi M, Sugahara T, et al. Metastable pitting and its correlation with electronic properties of passive films on Sn-xZn solder alloys. Corrosion Science. 2015;99:154-163.
44. Chan CW, Man HC, Yue TM. Effect of post-weld heat-treatment on the oxide film and corrosion behaviour of laser-welded shape memory NiTi wires. *Corrosion Science*. 2012;56:158-167.
45. Man HC, Cui ZD, Yue TM. Corrosion properties of laser surface melted NiTi shape memory alloy. *Scripta Materialia*. 2001;45(12):1447-1453.